

# SAX J1808.4–3658, an accreting millisecond pulsar shining in gamma rays?

E. de Oña Wilhelmi,<sup>1</sup> A. Papitto,<sup>1</sup> J. Li,<sup>1</sup> N. Rea,<sup>1,2</sup> D. F. Torres,<sup>1,3</sup>  
L. Burderi,<sup>4</sup> T. Di Salvo,<sup>5</sup> R. Iaria,<sup>5</sup> A. Riggio,<sup>4</sup> and A. Sanna<sup>4</sup>

<sup>1</sup>*Institute for Space Sciences (CSIC–IEEC), Campus UAB, Carrer de Can Magrans s/n, 08193 Barcelona, Spain*

<sup>2</sup>*Anton Pannekoek Institute for Astronomy, University of Amsterdam, Postbus 94249, NL-1090 GE Amsterdam, the Netherlands*

<sup>3</sup>*Institució Catalana de Recerca i Estudis Avançats (ICREA), 08010 Barcelona, Spain*

<sup>4</sup>*Università degli Studi di Cagliari, Dipartimento di Fisica, SP Monserrato-Sestu, KM 0.7, 09042 Monserrato, Italy*

<sup>5</sup>*Dipartimento di Fisica e Chimica, Università di Palermo, via Archirafi 36, 90123 Palermo, Italy*

Accepted XXX. Received YYY; in original form ZZZ

## ABSTRACT

We report the detection of a possible gamma-ray counterpart of the accreting millisecond pulsar SAX J1808.4–3658. The analysis of  $\sim 6$  years of data from the Large Area Telescope on board the *Fermi* Gamma-ray Space Telescope (*Fermi*-LAT) within a region of  $15^\circ$  radius around the position of the pulsar reveals a point gamma-ray source detected at a significance of  $\sim 6\sigma$  (Test Statistic TS = 32), with position compatible with that of SAX J1808.4–3658 within 95% Confidence Level. The energy flux in the energy range between 0.6 GeV and 10 GeV amounts to  $(2.1 \pm 0.5) \times 10^{-12}$  erg cm<sup>-2</sup> s<sup>-1</sup> and the spectrum is well-represented by a power-law function with photon index  $2.1 \pm 0.1$ . We searched for significant variation of the flux at the spin frequency of the pulsar and for orbital modulation, taking into account the trials due to the uncertainties in the position, the orbital motion of the pulsar and the intrinsic evolution of the pulsar spin. No significant deviation from a constant flux at any time scale was found, preventing a firm identification via time variability. Nonetheless, the association of the LAT source as the gamma-ray counterpart of SAX J1808.4–3658 would match the emission expected from the millisecond pulsar, if it switches on as a rotation-powered source during X-ray quiescence.

**Key words:** STARS: INDIVIDUAL: SAX J1808.4-3658, STARS: NEUTRON, GAMMA-RAYS: STARS

## 1 INTRODUCTION

Accretion-powered millisecond pulsars (AMSPs) are neutron stars (NSs) that orbit a low-mass companion star ( $\lesssim 1 M_\odot$ ) and show coherent X-ray pulsations at periods of a few milliseconds during X-ray flares known as outbursts, caused by the impact of an accretion stream onto the NS surface. The coherent pulsations observed in the X-ray light curve during outbursts are due to the channelling by the NS magnetosphere of (at least part of) the accretion flow to the magnetic poles of the NS.

SAX J1808.4–3658 was the first AMSP discovered (Wijnands & van der Klis 1998); since 1996, it has gone into a few-weeks long outburst eight times, i.e. roughly every 2.5 years (Patruno & Watts 2012 and references therein, and Sanna et al. 2015 for the most recent one) reaching a peak X-ray luminosity of a few times  $10^{36}$  erg s<sup>-1</sup>. During X-ray quiescence it shows a much fainter unpulsed X-ray emission, which attains a 0.5–10 keV luminosity ranging between 0.5

and  $1 \times 10^{32}$  erg s<sup>-1</sup> (Campana et al. 2002; Heinke et al. 2007).

Millisecond pulsars (MSPs) are believed to achieve their fast rotation during a Gyr-long phase of accretion of mass and angular momentum from a companion star (Alpar et al. 1982; Radhakrishnan & Srinivasan 1982). When the mass-transfer rate declines at the end of the accretion phase the NS magnetosphere is able to expand up to the light cylinder, and the pulsar switches on as an MSP powered by the rotation of its magnetic field. MSPs accelerate electron/positron pairs along field lines, driving a pulsed emission observed mainly in the radio and gamma-ray bands. The close link between accreting NSs and MSPs was recently demonstrated by the discovery of IGR J18245–2452, which during outburst was observed as an AMSP, after having been previously detected as a radio MSP during X-ray quiescence (Papitto et al. 2013). This source switches between these two states over a few weeks, presumably in response to variations of the mass in-flow rate (Stella et al.

1994; Campana et al. 2002; Burderi et al. 2003). Several indirect indications have been collected that a radio pulsar turns on during the quiescent state of other AMSPs. For SAX J1808.4–3658, in particular, the amount of optical light reprocessed by the companion star during X-ray quiescence (Homer et al. 2001) is compatible with irradiation by a radio pulsar (Burderi et al. 2009), the decrease of the NS spin period between consecutive outbursts is similar to the rate observed from MSPs (Hartman et al. 2009; Patruno et al. 2012), and the rapid increase of the orbital period suggests ejection of the mass transferred from the companion star and/or changes in the mass quadrupole moment of the companion (di Salvo et al. 2008; Burderi et al. 2009; Patruno et al. 2012). However, radio pulsations have not been detected from either SAX J1808.4–3658 or other AMSPs (Burgay et al. 2003; Iacolina et al. 2009, 2010), except for the case of IGR J18245–2453 (Papitto et al. 2013). This could be due to an intrinsic low luminosity of the radio pulsar, geometrical effects, and/or free-free absorption from material ejected from the system by the pulsar radiation pressure (di Salvo et al. 2008). Note that two more MSPs, PSR J1023+0038 (Archibald et al. 2009; Patruno et al. 2014) and XSS J12270–4859 (Bassa et al. 2014), have been observed in an intermediate state characterized by the presence of an outer accretion disk, and during which accretion-powered X-ray pulsations were detected (Archibald et al. 2014; Papitto et al. 2015). However the X-ray luminosity of these sources during such episodes ( $\approx 5 \times 10^{33}$  erg s<sup>-1</sup>) is much fainter than that usually attained by AMSPs, which possibly indicates that a large fraction of the mass in-flow is ejected by the quickly rotating NS magnetosphere rather than accreted onto the NS surface.

Turning to high energies (HE;  $100 \text{ MeV} < E < 100 \text{ GeV}$ ) is a promising strategy to detect the emission expected from an MSP turned on during the X-ray quiescent state of an AMSP. *Fermi*-LAT (Atwood et al. 2009) has proved to be an efficient rotation-powered MSP detector (Abdo et al. 2013) benefiting from the larger emission angle in gamma rays, and the absence of absorption from material possibly enshrouding the binary. The gamma-ray pulsar sample comprises not only canonical young pulsars but also recycled MSPs, that generally show a similar spectral shape as the young ones. The sky region of several AMSPs was already investigated by Xing & Wang (2013) to search for gamma-ray emission in the 100 MeV to 300 GeV range over a time span of 4 years, but they did not detect significant emission associated with any AMSP. A source compatible with the position of SAX J1808.4–3658 and dubbed 3FGL J1808.4–3703, is listed in the recently published *Fermi*-LAT 4-year point source catalogue (3FGL, Acero et al. 2015) with a detection significance of  $4.5\sigma$ . Also, a possible detection of the gamma-ray counterpart of SAX J1808.4–3658 was reported by Xing et al. (2015), who nevertheless searched for gamma-ray pulsations using only the nominal values of the ephemeris reported in Hartman et al. 2009, apparently overlooking the effect of the uncertainties on the position, orbital and spin parameters over the coherence of a signal searched in a few years-long time series. Here we analyze almost six years of LAT data from the region around SAX J1808.4–3658 to investigate the possibility of the source emitting a significant fraction of its energy in the gamma-ray regime. We performed a detailed timing analysis to search for periodic

features that could firmly identify the gamma-ray source as the counterpart of SAX J1808.4–3658, carefully treating the impact of the uncertainties of the system timing and spatial parameters on the range of parameters that have to be considered.

## 2 DATA ANALYSIS AND RESULTS

### 2.1 Data Analysis

To search for a gamma-ray counterpart of SAX J1808.4–3658 we analyzed data obtained with *Fermi*-LAT in a region of  $15^\circ$  radius around its position ( $\text{RA}_{\text{J2000}} = 18\text{h}08\text{m}27.62\text{s}$ ,  $\text{Dec}_{\text{J2000}} = -36^\circ 58'43.3''$ , Hartman et al. 2008). The LAT experiment on board the *Fermi Gamma-ray Space Telescope* satellite is sensitive to gamma rays with energies from 20 MeV to above 300 GeV, recording events with a timing accuracy better than  $1 \mu\text{s}$  (Abdo et al. 2009). Almost six years of data (*P7REP*, *SOURCE* class) obtained between the beginning of the operation MJD 54682.6 (August 4, 2008) and MJD 56812.4 (June 4, 2014) were processed using the publicly available *Fermi*-LAT Science Tools (software version v9r32p5), analyzed with the response functions *P7REP\_SOURCE\_V15* and using the templates for Galactic (*gLIem\_v05.fits*) and isotropic (*iso\_source\_v05.txt*) backgrounds. We selected data in the 100 MeV to 300 GeV energy range. Standard time event cuts performed with the tool *gtmktime* (*DATA\_QUAL*==1, *LAT\_CONFIG*==1 and *ABS(ROCK\_ANGLE)*<52) were applied. To suppress the effect of the Earth limb background, we excluded time intervals when the Earth was in the field of view (FoV, when the LAT Z-axis was more than  $52^\circ$  from zenith), and those in which part of the selected ROI was observed with zenith angle larger than  $100^\circ$ . A second analysis was performed excluding the periods in which SAX J1808.4–3658 was in an X-ray bright outburst state, i.e. between September 22nd and November 7th 2008 and November 5th to 20th 2011 (Hartman et al. 2009; Patruno et al. 2012), with compatible results to those presented next. No significant gamma-ray excess is detected when analysing time intervals when the source was in outburst.

### 2.2 Image and Spectral analysis

The image of the sky around the position of SAX J1808.4–3658 was obtained in the energy range above 1 GeV, where the angular resolution of *Fermi*-LAT reaches  $\approx 0.8^\circ$  on axis. Using the same exposure and instrument response from the data set, we modelled the region of interest (ROI) with all the 3FGL sources (Acero et al. 2015) (excluding 3FGL J1808.4–3703) and the standard Galactic and isotropic diffuse components and we let all the spectral parameters free (except for the spectra of the sources more than  $10^\circ$  away from the center) in a maximum likelihood fit (using *glike*<sup>2</sup>). Figure 1 shows the residuals with respect to the best-fit model. The residual image shows a point source compatible with the position of SAX J1808.4–3658 (see blue cross).

<sup>1</sup> [http://www.slac.stanford.edu/exp/glast/groups/canda/lat\\_Performance.htm](http://www.slac.stanford.edu/exp/glast/groups/canda/lat_Performance.htm)

<sup>2</sup> <http://fermi.gsfc.nasa.gov/ssc/data/analysis/scitools/>

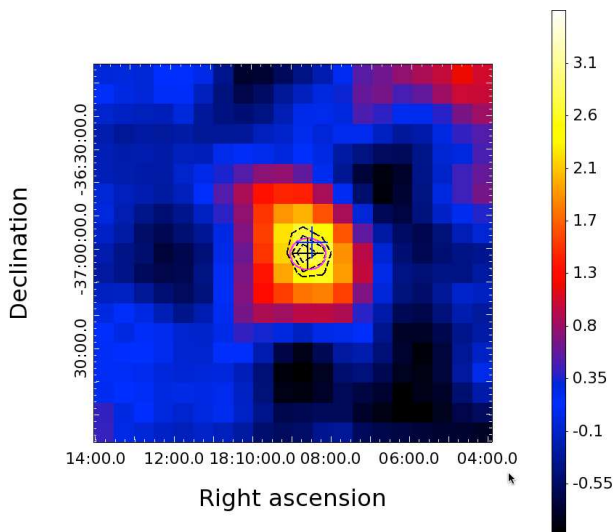


**Figure 1.** *Fermi*-LAT residual  $2^\circ \times 2^\circ$  (using a pixel size of  $0.1^\circ \times 0.1^\circ$ ) count map above 1 GeV of the SAX J1808.4–3658 region smoothed with a Gaussian of width  $\sigma = 0.3^\circ$  (units of the scale on the right are counts). The best-fit position of the gamma-ray source is marked with a black cross whereas the position of SAX J1808.4–3658 is marked in blue. The black-dashed lines show the TS significance contours above 1 GeV corresponding to CL of 68%, 95% and 99%. The magenta circle shows the 95% CL error in the best-fit position.

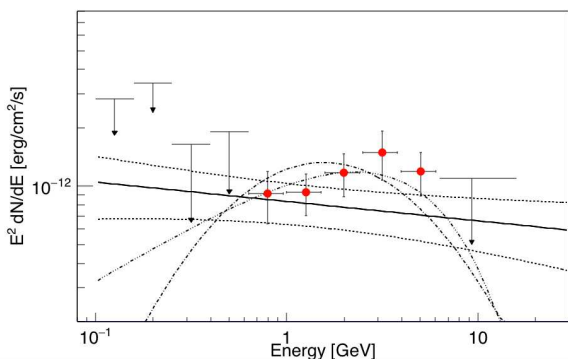


**Figure 2.** SED obtained at the position of SAX J1808.4–3658. The best-fit power law function is plotted as a solid line, and the dashed lines shows the statistical errors in the global fit. No highly significant improvement (by less than  $3\sigma$ ) is obtained using more sophisticated models, such as a power law with cut-off at high energies function or a log parabola function. The best-fit functions for the latter models are shown in dash-dot-dot and dash-dot lines, for exponential cutoff and log parabola functions respectively.

For the computation of the significance and spectral parameters of SAX J1808.4–3658 we added a point source at  $RA_{J2000} = 272.115^\circ$  and  $Dec_{J2000} = -36.98^\circ$  to account for the gamma-ray excess.

The inclusion of a point gamma-ray source at the position of SAX J1808.4–3658 described with a power-law function,  $\phi_0 \times (E/E_0)^{-\Gamma}$ , normalised at  $E_0 = 1.44$  GeV with  $\phi_0 = (2.42 \pm 0.56) \times 10^{-10}$   $\text{GeV}^{-1}\text{cm}^{-2}\text{s}^{-1}$  and  $\Gamma = 2.1 \pm 0.1$  (in black in Fig. 2), results in a test statistic (TS, [Mattox et al. 1996](#)) value of 31.6, which corresponds to a source detec-

tion at a confidence level of  $\sim 6\sigma$ . Applying the *point-like maximum-likelihood fitting* package ([Kerr 2010](#)) we fit the position of the gamma-ray excess above 100 MeV to  $RA_{J2000} = (272.143 \pm 0.037)^\circ$  and  $Dec_{J2000} = (-37.034 \pm 0.032)^\circ$  (compatible with the position of SAX J1808.4–3658 within 95% CL, see magenta circle in Fig. 1). The contour lines for 68, 95 and 99% Confidence Level (CL) obtained from the significance map, calculated with *gtlsmmap* for events above 1 GeV are also shown.

The spectral energy distribution (SED) for a point source centered on the position of SAX J1808.4–3658 was derived by means of a binned likelihood fitting, divided in 15 logarithmic bins between 100 MeV and 300 GeV (see Fig. 2). The spectral points obtained for each energy bin (with significance of more than  $2\sigma$ ), fitting the data with a power-law function with fixed photon index of 2, are shown in Fig. 2. More sophisticated spectral shapes, aiming to fit the 100 MeV to 300 GeV spectral range, do not provide a statistically-significant improvement to the fit. The comparison with a fit to a log parabola function ( $\phi = \phi_0(E/E_b)^{-(\alpha+\beta \log(E/E_b))}$ ) results in a difference in the maximum likelihood of  $2 \times \Delta L / \Delta(\text{ndf}) = 10$  (with  $\Delta(\text{ndf}) = 2$  and probability  $P = 6.7 \times 10^{-3}$ , corresponding to  $2.7\sigma$ ), whereas the comparison to a power-law function plus exponential cutoff ( $\phi = \phi_0(E/E_0)^{-\gamma} \exp(-E/E_c)$ ) leads to an increase of only 8 (with  $\Delta(\text{ndf}) = 1$  and probability  $P = 4.57 \times 10^{-3}$ , corresponding to  $2.8\sigma$ ). For the log parabola hypothesis, the best-fit parameters we found are  $\phi_0 = (4.20 \pm 0.32) \times 10^{-10}$   $\text{GeV}^{-1}\text{cm}^{-2}\text{s}^{-1}$ ,  $\alpha = 1.91 \pm 0.09$  and  $\beta = 0.41 \pm 0.02$  for a break energy of  $E_b = 1.4$  GeV, whereas when we try to fit to a power-law function plus exponential cutoff we obtain  $\phi_0 = (3.2 \pm 2.7) \times 10^{-8}$   $\text{GeV}^{-1}\text{cm}^{-2}\text{s}^{-1}$ ,  $\gamma = 1.4 \pm 0.4$  and  $E_c = 3.8 \pm 25$  GeV.

### 2.3 Timing analysis

The long term exposure-corrected (counts/exposure) light curve, produced by means of *aperture photometry* within a radius of  $1^\circ$  and retaining photons between 100 MeV and 300 GeV, does not show any deviation from a constant flux. The fit to a constant flux results in a  $\chi^2/\text{ndf}$  of 0.9 (for  $\text{ndf} = 210$ ) using a linear binning with a bin width of 10 days. In order to search for a modulation of the gamma-ray flux at the orbital period of the gamma-ray flux, we folded the light curve in 10 bins around the value of the orbital period predicted according to:

$$P_{orb}(t) = P_{orb}(T_0) + \dot{P}_{orb}(T_0) \times (t - T_0) + \frac{1}{2} \ddot{P}_{orb}(T_0) \times (t - T_0)^2, \quad (1)$$

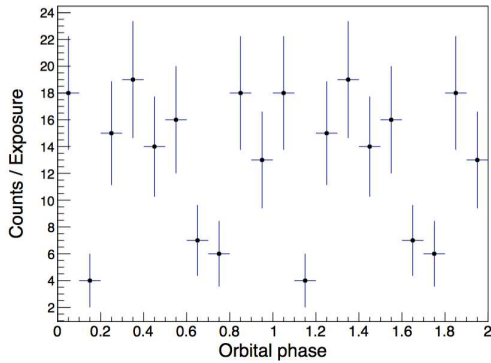
where  $T_0 = 54730$  MJD, and the values of  $P_{orb}(T_0)$ ,  $\dot{P}_{orb}(T_0)$  and  $\ddot{P}_{orb}(T_0)$  are listed in Table 1 ([di Salvo et al. 2008](#); [Burderi et al. 2009](#); [Patruno et al. 2012](#)). The variance of the folded profile extracted considering photons at energies larger than 100 MeV is  $\chi^2/\text{ndf} = 11/9$ , indicating no evidence of a significant modulation. A similar result is obtained considering only photons at higher energies (e.g.,  $> 2$  GeV). The fit to a constant function results in a  $\chi^2/\text{ndf}$  of 30/9 (see Fig. 3), corresponding to a marginal P-value of  $5 \times 10^{-4}$  pre-trial.

The search for gamma-ray pulsations is limited by the uncertainties in the ephemeris and position of the source and

**Table 1.** Parameters used in the periodicity search.

| Parameter   | Best estimate, $x_i$                  | Error, $\sigma_{x_i}$                 | Sensitivity, $\delta_{x_i}$          | No. corrections, $N_{x_i}$ |
|---|---------------------------------------|---------------------------------------|--------------------------------------|----------------------------|
| Ecliptic longitude, $\lambda$                       | 271.737918°                           | 0.13''                                | 0.015''                              | 16                         |
| Ecliptic latitude, $\beta$                          | -13.552162°                           | 0.15''                                | 0.064''                              | 5                          |
| Orbital period, $P_{orb}(T_0)$                      | 7249.157964 s                         | $7.6 \times 10^{-5}$ s                | $3.4 \times 10^{-4}$ s               | 1                          |
| Orbital period derivative, $\dot{P}_{orb}(T_0)$     | $3.17 \times 10^{-12}$                | $0.70 \times 10^{-12}$                | $1.8 \times 10^{-12}$                | 1                          |
| Orbital period second deriv., $\ddot{P}_{orb}(T_0)$ | $1.65 \times 10^{-20} \text{ s}^{-1}$ | $0.35 \times 10^{-20} \text{ s}^{-1}$ | $2.0 \times 10^{-20} \text{ s}^{-1}$ | 1                          |
| Epoch of passage at asc. node, $T^*$                | 54729.999079 MJD                      | 0.78 s                                | 14.9 s                               | 1                          |
| Semi-major projected axis, $a \sin i/c$             | 62.812 lt-ms                          | $2 \times 10^{-3}$ lt-ms              | 2.0 lt-ms                            | 1                          |
| Spin frequency, $\nu(T_0)$                          | 400.97521014 Hz                       | $2.4 \times 10^{-2} \mu\text{Hz}$     | $5.4 \times 10^{-3} \mu\text{Hz}$    | 27                         |
| Spin frequency derivative, $\dot{\nu}$              | $7.1 \times 10^{-16} \text{ Hz/s}$    | $-1.2 \times 10^{-16} \text{ Hz/s}$   | $3.3 \times 10^{-17} \text{ Hz/s}$   | 25                         |

Notes: Position and orbital parameters were taken from [Hartman et al. \(2008, 2009\)](#) and [Patruno et al. \(2012\)](#). Frequency and frequency derivative were measured by fitting the spin frequency values given by [Hartman et al. \(2008, 2009\)](#); [Patruno et al. \(2012\)](#) with a constant spin-down function (see black dashed line in Fig. 4). The reference epoch is  $T_0 = \text{MJD } 54730$ . The total observation time is  $T_{obs} = 2129.8$  d. See Sec. 2.2 for details on the assessment of the sensitivity to a coherent signal over the considered time series.

**Figure 3.** Phaseogram obtained folding the arrival time of the exposure-corrected gamma-ray photons  $E > 2$  GeV with the orbital period  $P_{orb}(t)$  obtained from equation 1.

the (faint) flux level detected. This search must take into account the loss of signal coherency over the  $T_{obs} = 2129.8$  d-long interval spanned by the observations. The following effects are considered, (i) the orbital motion of the pulsar, (ii) the intrinsic evolution of the pulsar spin, and (iii) uncertainties on the position of the source.

The frequency variations induced by the orbital motion of the source have to be taken into account by correcting the photon arrival times to the line of nodes of the binary system, using the most updated orbital solution available (see Table 1). Assuming that the orbital period evolution is described by Eq. 1, the maximum uncertainty on the estimate of the orbital period driven by the errors on the values of  $P_{orb}(T_0)$ ,  $\dot{P}_{orb}(T_0)$  and  $\ddot{P}_{orb}$ , is evaluated by standard error propagation over the length of the considered time series:

$$\sigma_{P_{orb}}^{max} = \left[ \sigma_{P_{orb}}^2 + (\sigma_{\dot{P}_{orb}} T_{obs})^2 + \left( \frac{1}{2} \sigma_{\ddot{P}_{orb}} T_{obs}^2 \right)^2 \right]^{1/2} = 1.6 \times 10^{-4} \quad (2)$$

In order to check if the actual uncertainties on the orbital parameters produce a loss of coherence of the pulsar signal, we used the expressions given by [Caliandro et al. \(2012\)](#), see Table 3 therein), who estimated the fraction of power lost,  $\epsilon$ , as a function of the difference between the actual value of an orbital parameter and the one used to refer photon

times of arrival to the line of nodes of the binary system. We evaluated the analytical relations they give for the case of a circular orbit:

$$\delta(a \sin i/c) = \frac{1}{2\nu_0} \frac{1}{\epsilon^2} \quad (3)$$

$$\delta T^* = \frac{0.1025 P_{orb}}{\pi \nu_0 (a \sin i/c)} \frac{1}{\epsilon^2} \quad (4)$$

$$\delta P_{orb} = \frac{P_{orb}^2}{2\pi \nu_0 (a \sin i/c) T_{obs}} \sqrt{\left( \frac{1-\epsilon^2}{10} \right)}, \quad (5)$$

for  $\epsilon = 0.8$ , obtaining the values listed in Table 1 in the column labelled as ‘Sensitivity’. Here,  $a \sin i/c$  is the projected semi-major axis of the NS orbit, and  $T^*$  is the epoch of passage of the NS at the ascending node of the orbit. For each of the orbital parameters,  $x_i$ , the sensitivity value  $\delta_{x_i}$  is larger than the uncertainty  $\sigma_{x_i}$  (see Table 1), assuring that signal coherence is not lost throughout the length of the considered observation. The sensitivity to the uncertainty on the value of the first and second derivative of the orbital period were evaluated by taking the value that alone would produce a period shift equal to  $\delta P_{orb}$ , namely,  $\delta \dot{P}_{orb} = \delta P_{orb}/T_{obs}$  and  $\delta \ddot{P}_{orb} = 2\delta P_{orb}/T_{obs}^2$  (see Eq. 1).

So far, coherent pulsations were detected from SAX J1808.4–3658 only in the X-ray light curves observed during six of the outbursts shown by the source since 1998, each of which lasted a few weeks. We extrapolated the spin evolution of the pulsar, fitting a constant spin-down model to the frequencies measured in different outbursts. In addition, the measure of the spin frequency of SAX J1808.4–3658 during each of the outbursts is complicated by the presence of strong timing noise that exceeds Poisson counting noise and affects, to a different extent, the first and second harmonic of the signal ([Burderi et al. 2009](#)). [Hartman et al. \(2009\)](#) and [Patruno et al. \(2012\)](#) measured the frequency of the signal during each of the outbursts using a frequency-domain filter to weigh the harmonics according to the observed noise properties and estimated the uncertainty by performing Monte Carlo simulations. Using this method they found no significant evolution of the spin frequency during the various outbursts. Here we consider the spin frequency that they measured in each of the outbursts, summing in quadrature the uncertainty driven by positional errors  $\delta \nu_{pos}^{max}$  (see below) to the uncertainty quoted on their values. By fitting the average frequency values observed during the six different outbursts

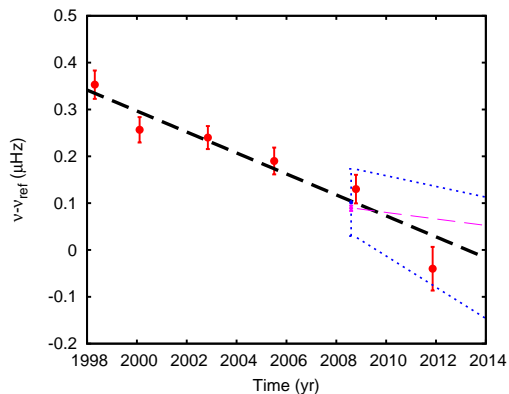


**Figure 4.** Evolution of the spin frequency of SAX J1808.4–3658 as observed in the X-ray band. The dashed black line is the best-fitting spin-down trend, the dotted blue lines mark the range of parameters searched, and the magenta line is the solution that gives the maximum H-test value. The reference frequency is  $\nu_o = 400.975210$  Hz.

with a constant spin-down trend,

$$\nu(t) = \nu(T_0) + \dot{\nu} \times (t - T_0), \quad (6)$$

we estimated the spin frequency derivative as  $\dot{\nu} = (7.1 \pm 1.2) \times 10^{-16}$  Hz s $^{-1}$  (see dashed line in Fig. 4), compatible with the value given by Patruno et al. (2012). Propagating the errors on the spin frequency and its derivative over the whole length of the observations leads to a maximum uncertainty on the signal frequency of

$$\sigma_{\nu}^{max} = [\sigma_{\nu}^2 + (\sigma_{\dot{\nu}} T_{obs})^2]^{1/2} \simeq 3 \times 10^{-2} \mu\text{Hz}. \quad (7)$$

We assume that the minimum difference between frequencies that produces a significant power loss in a search for a signal is equal to the independent Fourier frequency spacing,  $\Delta\nu_{IFS} = 1/T_{obs} = 5.4 \times 10^{-3}$   $\mu\text{Hz}$ . As the maximum uncertainty on the spin frequency  $\sigma_{\nu}^{max}$  is larger than  $\Delta\nu_{IFS}$ , we are forced to perform a search over different possible values of  $\nu(T_0)$  and  $\dot{\nu}$  in order to avoid a significant loss of signal power. We varied the spin frequency and its derivative in steps equal to the amount that produces an uncertainty equal to  $\Delta\nu_{IFS}$  over a time interval equal to  $T_{obs}$ , i.e.  $\delta\nu = \Delta\nu_{IFS} = 5.4 \times 10^{-3}$   $\mu\text{Hz}$ , and  $\delta\dot{\nu} = \Delta\nu_{IFS}/T_{obs} = 1/T_{obs}^2 = 2.9 \times 10^{-17}$  Hz/s. In order to cover an interval equal to  $\pm 3\sigma$  around the central value of  $\nu(T_0)$  and  $\dot{\nu}$ , we then performed  $N_{\nu} = 2 \times (3\sigma_{\nu})/\delta\nu = 27$  and  $N_{\dot{\nu}} = 2 \times (3\sigma_{\dot{\nu}})/\delta\dot{\nu} = 25$  correction trials on the spin frequency and its derivative, respectively. The limits of the range of values covered is plotted in Fig. 4 using blue dashed lines.

An additional number of correction trials has to be performed when photon arrival times are converted to the Solar System barycenter, because of the uncertainty on the source position. We considered the position of the optical counterpart determined by Hartman et al. (2009), RA = 18h08m27.62s, DEC =  $-36^{\circ}58'43.3''$ , with an uncertainty of  $0.15''$  [corresponding to ecliptic coordinates  $\lambda = 271.737918^{\circ}$ ,  $\beta = -13.552162^{\circ}$ , affected by uncertainties  $\sigma_{\lambda} = 0.13''$ , and  $\sigma_{\beta} = 0.15''$ , respectively (see Table 1)]. A difference of  $(\delta\lambda, \delta\beta)$  between the actual ecliptic coordinates of the source  $(\lambda, \beta)$ , and those used to correct the time series, yields an apparent modulation of the spin frequency

of the signal equal to:

$$\delta\nu_{pos} = \nu y \left( \frac{2\pi}{P_{\oplus}} \right) [\cos A_0 \cos\beta \delta\lambda + \sin A_0 \sin\beta \delta\beta] \quad (8)$$

(Manchester & Peters 1972). Here  $y$  is the Earth distance from the Solar System barycenter,  $P_{\oplus} = 1$  yr,  $A_0 = [2\pi(T_0 - T_{\gamma})/P_{\oplus}]$ ,  $T_0$  is the start time of observations and  $T_{\gamma}$  is the Vernal point. Considering that our time-series covers  $\simeq 5.8$  yr, the uncertainty on the position of SAX J1808.4–3658 translates into a modulation of the signal frequency of amplitude  $\delta\nu_{pos}^{max} \simeq 2.4 \times 10^{-2}$   $\mu\text{Hz}$ . As for the uncertainty on the spin frequency and its derivative (see above), this value is also larger than the spacing between independent Fourier frequencies,  $\Delta\nu_{IFS} = 5.4 \times 10^{-3}$   $\mu\text{Hz}$ , forcing us to perform a series of corrections on the coordinates used to barycenter the *Fermi*-LAT light curve. We estimated the minimum difference between coordinates that produces a significant signal loss as that producing a frequency oscillation  $\delta\nu_{pos}$  (evaluated using Eq. 8 and putting  $\cos A_0$  and  $\sin A_0$  equal to one, for simplicity) equal to  $\Delta\nu_{IFS}$ . We thus obtained  $\delta\lambda = 0.015''$  and  $\delta\beta = 0.064''$ . In order to cover a range within  $1\sigma$  from the central estimates of the source coordinates,  $N_{\lambda} = 2\sigma_{\lambda}/\delta\lambda = 16$  and  $N_{\beta} = 2\sigma_{\beta}/\delta\beta = 5$  preliminary corrections of the time series were then performed (see Table 1, where the parameters of the grid used in the periodicity search are given). That implies  $N_{\lambda}N_{\beta} = 80$  time series, for which  $N_{\nu}N_{\dot{\nu}} = 675$  searches over  $\nu$  and  $\dot{\nu}$  should be performed. Considering the flux level of the detected source (with  $\sim 100$  photons detected from the source direction), the total number of trials needed to apply ( $N_{tr} = 54000$ ) strongly hampers the search for gamma-ray pulsations at the spin period of the source, given the current uncertainties and instrument sensitivity. Considering these values, only a signal with a sinusoidal amplitude  $\gtrsim 65\%$  (i.e. giving a  $\chi^2/(\text{ndf} - 1) = 5.75$  for  $\text{ndf} = 10$ ) would be detected at  $3\sigma$  confidence level by an epoch folding search technique, performed by sampling the profile with  $\text{ndf} = 10$  phase bins (Leahy 1987)<sup>3</sup>

Nevertheless, we searched for a periodic signal in the *Fermi*-LAT light curve in the range considered in Fig. 4. The arrival time of each event was first transformed to the Solar System barycenter using the grid of positions determined previously, then we applied the corrections for the orbital motion, and finally we calculated the phase of each photon using the grid of values of frequency and frequency derivative determined above. The time correction was done using the LAT *gtpphase* tool. The uniformity of the phaseogram is tested by both applying a simple epoch folding search test on a 10-bin pulse profile and an H-test (de Jager & Büsching 2010) on the arrival events. Fig. 5a shows the distribution of the  $\chi^2$  obtained with an epoch folding search for different positions,  $\nu$  and  $\dot{\nu}$ . The two tests reached a maximum of their value  $\chi^2/\text{ndf} = 3.8$  (with  $\text{ndf} = 9$ ) and  $H = 11.7$  for  $m = 2$ , where  $m$  is the number of harmonics used when the data set is folded using the combination of  $\lambda_0 = 271.737942^{\circ}$ ,  $\beta_0 = -13.552197^{\circ}$ ,  $\nu_0 = 400.975210089$  Hz and  $\dot{\nu}_0 = -2.2 \times 10^{-16}$  Hz/s. We performed the same statistics test around

<sup>3</sup> We note that the sensitivity to a signal with a lower duty-cycle, like those often observed from radio pulsars would be higher than in the case of a sinusoidal signal.

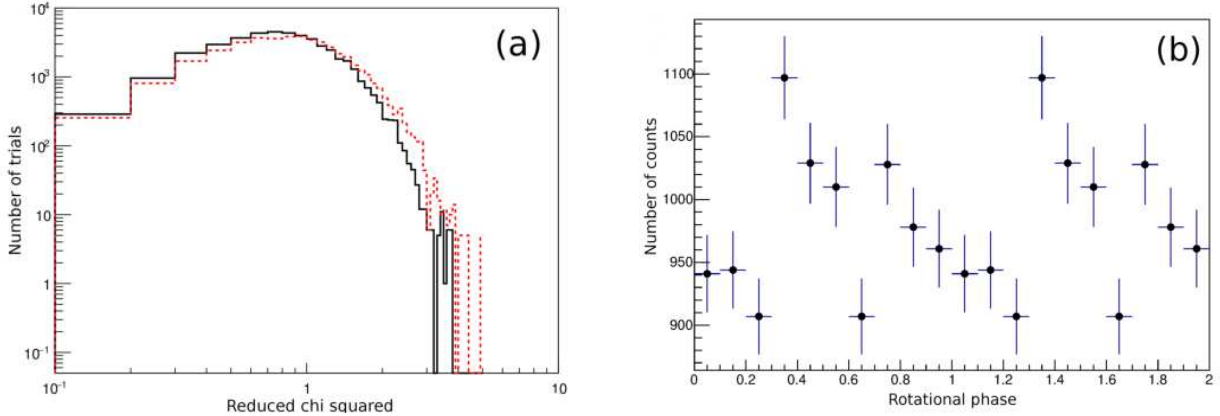


**Figure 5.** Left a)  $\chi^2/\text{ndf}$  distribution for positions, independent frequencies and frequency derivatives tested in a range of  $3\sigma$  around the expected  $\nu$  and  $\dot{\nu}$  and of  $1\sigma$  around the central estimate of the coordinates. The black distribution shows the results when using the correct ephemeris whereas the red one refers to the *fake* ones. Right b) Phaseogram obtained folding the arrival time of the gamma-ray photons with  $\nu_0$  and  $\dot{\nu}_0$  and on the position  $\lambda_0$  and  $\beta_0$ , which results in a maximum in the two periodicity tests applied. Two cycles are plotted for clarity, and y-axis is zero-suppressed.

*fake* values of  $\nu$  and  $\dot{\nu}$  ( $\nu_{\text{fake}} = 399.97521013$  Hz and  $\dot{\nu}_{\text{fake}} = -5.5 \times 10^{-16}$  Hz/s) to validate the uniformity of the test (in red in Fig. 5a). [de Jager & Büsching \(2010\)](#) showed that the probability distribution for the H-test can be described by  $P(> H) = \exp(-0.4H)$ . From this expression we can derive a probability of  $P(> 11.7) = 9.3 \times 10^{-3}$  before trials for the light curve to deviate from a flat distribution. The folded light curve obtained with  $\nu_0$  and  $\dot{\nu}_0$  and the position  $(\lambda_0, \beta_0)$  is shown in Fig. 5b (two cycles are plotted for clarity), and the relevant source spin evolution is plotted as a magenta dashed line in Fig. 4. Also considering the large number of trials made ( $N_{tr} = 54000$ ) such a solution is not significant. Similarly, the probability of obtaining a chi-squared value of  $\chi^2/\text{ndf} = 3.8$  for  $\text{ndf} = 9$  in a single epoch-folding is  $P = 8.2 \times 10^{-5}$ . Considering all the trials made, we expect  $N_{tr} \times P \simeq 4.4$  folded profiles to yield such a chi-squared value by chance, which indicates clearly that the detection is not significant.

### 3 DISCUSSION

The best-fit position of the gamma-ray source discovered is located  $3.2'$  from the optical position of SAX J1808.4–3658 (within the 95% CL of the gamma-ray source position). We investigated a region of  $0.15^\circ$  radius surrounding the position of the gamma-ray source, and no obvious possible gamma-ray-producing counterpart or gamma-ray accelerator was found beside the AMSP. The only source detected in the surrounding is the radio galaxy NVSS 180824–365813 ([Condon et al. 1998](#)), although the lack of an X-ray counterpart and faint flux make it an unlikely candidate to emit in gamma rays ([Beckmann et al. 2014](#)). A more detailed investigation of faint X-ray sources other than SAX J1808.4–3658 can be found in [Xing et al. \(2015\)](#).

In the 3FGL catalogue, a source compatible with the position of SAX J1808.4–3658 and dubbed 3FGL J1808.4–3703 is listed. Its flux and spectral parameters are compatible with the source reported here. [Xing et al.](#)

(2015) reported similar investigations. Nevertheless a search for gamma-ray pulsations was done by the previous authors without taking into account the possible range of possible ephemeris. [Xing et al. \(2015\)](#) also reported a barely significant modulation at the orbital period. Here, a detailed timing analysis is performed, considering the uncertainties of the system timing and spacial parameters. We also checked that their result could be reproduced (with a statistical significance in the 10 bins light-curve of  $\chi^2/\text{ndf} = 30/9$ , corresponding to  $3.5\sigma$ ) only by extracting photons with energies  $> 2$  GeV, coming from a region around  $0.6^\circ$  around the source. The non-detection of any significant modulation when considering a region of different size or a different energy band raises doubts on the reliability of such a claim.

If the identification of the gamma-ray source found with the AMSP is real, the gamma-ray emission could originate either in the pulsar magnetosphere or in the intra-binary shock. No significant variation at the time scale set by the orbital period has been found. We also folded the arrival times of the gamma-ray photons around the spin frequency of the pulsar, using the latest ephemeris measured during the last flaring state, and allowing a deviation of  $3\sigma$  with respect to the extrapolated value for  $\nu$  and  $\dot{\nu}$ . The position of the source was also varied to take into account the error in the position determination when converting to the Solar System barycenter. Considering the large number of trials needed to cover all the possible spin and position parameters, no significant detection of gamma-ray pulsations could be achieved. Even though we can not yet formally identify the LAT source with SAX J1808.4–3658 we can compute the gamma-ray luminosity for a scenario in which SAX J1808.4–3658 is producing the detected gamma-ray radiation at a distance of  $3.5 \pm 0.1$  kpc ([Galloway & Cumming 2006](#)). We obtain a total luminosity of  $L_\gamma = (3 \pm 1) \times 10^{33}$  erg/s in the energy range between 0.6 GeV and 10 GeV (i.e., the energy range in which the source was significantly detected, see Fig. 2), which is compatible with upper limits obtained previously by [Xing & Wang \(2013\)](#) in a search of gamma-ray counterpart of several AMSP, including SAX J1808.4–

3658. If we compare with the total rotational power at present ( $\dot{E} = (1.1 \pm 0.2) \times 10^{34}$  erg/s obtained from the values of  $\nu$  and  $\dot{\nu}$  quoted in Table 1 and using a moment of inertia of  $10^{45}$  g cm<sup>2</sup>) assuming a beaming factor of  $f_{\Omega} = 1$  (Watters et al. 2009), we obtain an efficiency of  $\eta = L_{\gamma}/\dot{E} \times 100 = (27 \pm 9)\%$ , which is within the range of efficiencies observed from MSPs detected at high energy (Espinoza et al. 2013; Guillemot 2009; Ray et al. 2013; Abdo et al. 2013). If the association can finally be proven, SAX J1808.4–3658 in X-ray quiescence will be similar to PSR J1311–3430 (Pletsch et al. 2012; Ray et al. 2013), a fast MSP ( $\approx 2.5$  ms) in a compact binary system ( $\approx 2$  h). The spectral parameters are also compatible within the current statistics to the ones found in other MSPs, with a hard spectrum and a turn over at a few GeV (Espinoza et al. 2013; Abdo et al. 2013).

Two MSPs, PSR J1023+0038 and XSS J12270–4859, have recently been observed to switch between a rotation-powered radio pulsar state and an intermediate state characterized by the presence of an outer accretion disk. In the disk state these two sources showed a 0.1–100 GeV gamma-ray luminosity of a few  $\times 10^{34}$  erg s<sup>−1</sup> (de Martino et al. 2010; Hill et al. 2011; Stappers et al. 2014), larger by up to an order of magnitude than the gamma-ray luminosity shown in the radio pulsar state. The brighter gamma-ray output observed from MSPs in the intermediate disk state has been interpreted in terms of an intra-binary shock close to the pulsar (Stappers et al. 2014; Coti Zelati et al. 2014), inverse-Compton scattering of UV disk photons by the pulsar wind (Takata et al. 2014; Li et al. 2014), and synchrotron self-Compton emission from the inner disk boundary around a propelling NS (Papitto et al. 2014b). On the other hand, the lower luminosity observed from the proposed counterpart of SAX J1808.4–3658 is similar to that usually observed from MSPs in the rotation-powered state, and indicates that this is the most likely state in which SAX J1808.4–3658 lies during X-ray quiescence.

A detection of gamma-ray pulsations from SAX J1808.4–3658 would imply rotational-powered activity in quiescence mode, whereas for SAX J1808.4–3658 pulsed emission due to accretion-power mechanisms was detected during the bursting accretion phase. If confirmed, SAX J1808.4–3658 will add to IGR J18245–2452 (Papitto et al. 2013), PSR J1023+0038 (Archibald et al. 2014) and XSS J12270–4859 (Papitto et al. 2014a) as a source showing evidence of a transition to a rotation-powered radio pulsar state in X-ray quiescence, whilst it is observed as an accreting pulsar when it has a disk. That would also emphasise the potential of the gamma-ray regime to investigate these systems, avoiding observational biases suffered in other bands, such as large absorption or narrow radio beams.

## 4 CONCLUSIONS

In a search for a gamma-ray counterpart for SAX J1808.4–3658 we discovered a weak gamma-ray source when analyzing almost six years of data obtained with the LAT experiment. The position of the source is compatible within 3.2′ with the location of SAX J1808.4–3658. The LAT source exhibits an energy flux of  $(2.1 \pm 0.5) \times 10^{-12}$  erg cm<sup>−2</sup> s<sup>−1</sup> (in

the 0.6 GeV to 10 GeV energy range) and a point morphology.

The positional alignment between the gamma-ray source and SAX J1808.4–3658 and the lack of gamma-ray accelerators other than the AMSP suggest an association between the two. However the uncertainties in the position and rotational ephemeris of SAX J1808.4–3658 prevent a firm identification through phase variability. The uncertainty on the spin and spin frequency derivative will be improved by X-ray studies of the pulsations of the source during its future X-ray outbursts. On the other hand, the positional error is dominated by the 0.15′′ uncertainties on the 2MASS catalogue (Skrutskie et al. 2006) used to register the image of the optical counterpart of SAX J1808.4–3658 (Hartman et al. 2008), and will hopefully be improved by future missions devoted to astrometry.

## ACKNOWLEDGEMENTS

Work done in the framework of the grants AYA2012-39303, SGR2009–811 and SGR2012–1073. N. R. acknowledges support from an NWO Vidi Award, and NewCOMPSTAR COST Action MP1304. A. R. acknowledges Sardinia Regional Government for financial support (P.O.R. Sardegna F.S.E. Operative Programme of the Autonomous Region of Sardinia, European Social Fund 2007-2013 - Axis IV Human Resources, Objective I.3, Line of Activity I.3.1). J.L. and D.F.T. acknowledge support from the National Natural Science Foundation of China via NSFC-11473027. D.F.T. further acknowledges the Chinese Academy of Sciences visiting professorship program 2013T2J0007.

The *Fermi* LAT Collaboration acknowledges generous ongoing support from a number of agencies and institutes that have supported both the development and the operation of the LAT as well as scientific data analysis. These include the National Aeronautics and Space Administration and the Department of Energy in the United States, the Commissariat à l’Energie Atomique and the Centre National de la Recherche Scientifique / Institut National de Physique Nucléaire et de Physique des Particules in France, the Agenzia Spaziale Italiana and the Istituto Nazionale di Fisica Nucleare in Italy, the Ministry of Education, Culture, Sports, Science and Technology (MEXT), High Energy Accelerator Research Organization (KEK) and Japan Aerospace Exploration Agency (JAXA) in Japan, and the K. A. Wallenberg Foundation, the Swedish Research Council and the Swedish National Space Board in Sweden.

Additional support for science analysis during the operations phase is gratefully acknowledged from the Istituto Nazionale di Astrofisica in Italy and the Centre National d’Études Spatiales in France.

## REFERENCES

- Abdo A. A., et al., 2009, *Astroparticle Physics*, **32**, 193
- Abdo A. A., et al., 2013, *ApJS*, **208**, 17
- Acero F., et al., 2015, preprint, ([arXiv:1501.02003](https://arxiv.org/abs/1501.02003))
- Alpar M. A., Cheng A. F., Ruderman M. A., Shaham J., 1982, *Nature*, **300**, 728
- Archibald A. M., et al., 2009, *Science*, **324**, 1411
- Archibald A. M., et al., 2014, preprint, ([arXiv:1412.1306](https://arxiv.org/abs/1412.1306))

- Atwood W. B., et al., 2009, *ApJ*, **697**, 1071
- Bassa C. G., et al., 2014, *MNRAS*, **441**, 1825
- Beckmann V., Soldi S., De Jong S., 2014, in 40th COSPAR Scientific Assembly. Held 2-10 August 2014, in Moscow, Russia, Abstract E1.5-16-14.. p. 239
- Burderi L., Di Salvo T., D'Antona F., Robba N. R., Testa V., 2003, *A&A*, **404**, L43
- Burderi L., Riggio A., di Salvo T., Papitto A., Menna M. T., D'Ai A., Iaria R., 2009, *A&A*, **496**, L17
- Burgay M., Burderi L., Possenti A., D'Amico N., Manchester R. N., Lyne A. G., Camilo F., Campana S., 2003, *ApJ*, **589**, 902
- Caliandro G. A., Torres D. F., Rea N., 2012, *MNRAS*, **427**, 2251
- Campana S., et al., 2002, *ApJ*, **575**, L15
- Condon J. J., Cotton W. D., Greisen E. W., Yin Q. F., Perley R. A., Taylor G. B., Broderick J. J., 1998, *AJ*, **115**, 1693
- Coti Zelati F., et al., 2014, *MNRAS*, **444**, 1783
- Espinoza C. M., et al., 2013, *MNRAS*, **430**, 571
- Galloway D. K., Cumming A., 2006, *ApJ*, **652**, 559
- Guillemot L., 2009, preprint, ([arXiv:0910.4707](https://arxiv.org/abs/0910.4707))
- Hartman J. M., et al., 2008, *ApJ*, **675**, 1468
- Hartman J. M., Patruno A., Chakrabarty D., Markwardt C. B., Morgan E. H., van der Klis M., Wijnands R., 2009, *ApJ*, **702**, 1673
- Heinke C. O., Jonker P. G., Wijnands R., Taam R. E., 2007, *ApJ*, **660**, 1424
- Hill A. B., et al., 2011, *MNRAS*, **415**, 235
- Homer L., Charles P. A., Chakrabarty D., van Zyl L., 2001, *MNRAS*, **325**, 1471
- Iacolina M. N., Burgay M., Burderi L., Possenti A., di Salvo T., 2009, *A&A*, **497**, 445
- Iacolina M. N., Burgay M., Burderi L., Possenti A., di Salvo T., 2010, *A&A*, **519**, A13
- Kerr M., 2010, PhD thesis, University of Washington
- Leahy D. A., 1987, *A&A*, **180**, 275
- Li K. L., Kong A. K. H., Takata J., Cheng K. S., Tam P. H. T., Hui C. Y., Jin R., 2014, *ApJ*, **797**, 111
- Manchester R. N., Peters W. L., 1972, *ApJ*, **173**, 221
- Mattox J. R., et al., 1996, *ApJ*, **461**, 396
- Papitto A., et al., 2013, *Nature*, **501**, 517
- Papitto A., de Martino D., Belloni T. M., Burgay M., Pellizzoni A., Possenti A., Torres D. F., 2014a, preprint, ([arXiv:1412.4252](https://arxiv.org/abs/1412.4252))
- Papitto A., Torres D. F., Li J., 2014b, *MNRAS*, **438**, 2105
- Papitto A., de Martino D., Belloni T. M., Burgay M., Pellizzoni A., Possenti A., Torres D. F., 2015, *MNRAS*, **449**, L26
- Patruno A., Watts A. L., 2012, preprint, ([arXiv:1206.2727](https://arxiv.org/abs/1206.2727))
- Patruno A., Bult P., Gopakumar A., Hartman J. M., Wijnands R., van der Klis M., Chakrabarty D., 2012, *ApJ*, **746**, L27
- Patruno A., et al., 2014, *ApJ*, **781**, L3
- Pletsch H. J., et al., 2012, *Science*, **338**, 1314
- Radhakrishnan V., Srinivasan G., 1982, *Current Science*, **51**, 1096
- Ray P. S., et al., 2013, *ApJ*, **763**, L13
- Sanna A., et al., 2015, *The Astronomer's Telegram*, 7364, 1
- Skrutskie M. F., et al., 2006, *AJ*, **131**, 1163
- Stappers B. W., et al., 2014, *ApJ*, **790**, 39
- Stella L., Campana S., Colpi M., Mereghetti S., Tavani M., 1994, *ApJ*, **423**, L47
- Takata J., et al., 2014, *ApJ*, **785**, 131
- Watters K. P., Romani R. W., Weltevrede P., Johnston S., 2009, *ApJ*, **695**, 1289
- Wijnands R., van der Klis M., 1998, *Nature*, **394**, 344
- Xing Y., Wang Z., 2013, *ApJ*, **769**, 119
- Xing Y., Wang Z., Jithesh V., 2015, preprint, ([arXiv:1502.00733](https://arxiv.org/abs/1502.00733))
- de Jager O. C., Büsching I., 2010, *A&A*, **517**, L9
- de Martino D., et al., 2010, *A&A*, **515**, A25
- di Salvo T., Burderi L., Riggio A., Papitto A., Menna M. T., 2008, *MNRAS*, **389**, 1851